Physica B: Condensed Matter 545 (2018) 465–474

Contents lists available at ScienceDirect

Physica B: Condensed Matter

journal homepage: www.elsevier.com/locate/physb

Kinetics of photodegradation mechanisms in organic photovoltaics

Muhammad Azeem Arshad, AbdelKrim Maaroufi*

University of Mohammed V, Faculty of Sciences, Department of Chemistry, Laboratory of Composite Materials, Polymers and Environment, Ibn Batouta Avenue, P.O. Box 1014, Rabat, Morocco

ARTICLE INFO

Keywords:
Organic photovoltaics
Kinetics
Photodegradation mechanism

ABSTRACT

Photodegradation is one of the burning issues in organic photovoltaics (OPV). It is also an obstacle in the commercialization of organic photovoltaic devices. Indeed, mechanistic approaches might satisfactorily address the stated issues by providing insights into the mechanisms of photodegradation processes in OPV. Albeit, while photodegradation mechanisms are of significant importance in OPV, a systematic approach to kinetically interpret those mechanisms has not yet been reported in the literature. In this regard, this paper puts forward a systematic and advanced kinetic approach comprising a set of mathematical models based on theoretical underpinning of photodegradation mechanisms taking place in OPV. The soundness of suggested kinetic approach is effectively tested on single-step as well as multi-step processes under various temperature conditions. A detailed account of the mechanistic predictions by employing the proposed kinetic approach is given and discussed in the present study. Certain prospective applications of the proposed approach are also considered.

1. Introduction

It is predicted by the energy experts that world would need 30 TW of energy by the mid of the century to maintain economic growth [1]. The relevant energy reservoirs must include a minimal fraction of fossil fuels as they cause raising the levels of greenhouse gas (CO_2) in the earth's atmosphere, which might eventually result in climate change [2]. It is noteworthy that certain serious attempts have recently been made to cope with the motioned environmental issue [3]. Therefore, in order to satisfy this substantial demand of energy, a significant portion of alternate energy resources is anticipated from renewable energies which are known for their relative abundance and eco-friendliness. Among these foreseen alternative resources of energy, solar energy is the most abundant renewable energy source. More than eighty five percent of solar cells occupying global photovoltaic market today are based on silicon [4,5]. Although, the reported efficiencies of such conventional solar cells are higher, yet their contribution is merely 0.05% in satisfying the global energy demand. The reason is that, the cost of solar energy conversion into electricity by expensive materials and energy demanding processing techniques is approximately the same as burning fossil fuels [6]. As a potential substitute, the organic photovoltaic cells (OPVCs) are the subject of a number of ongoing renewable energy researches due to their low cost, easy processing, and flexible energy source [7–13]. Nevertheless, there are still several challenges associated with these materials that remain to be addressed for their large scale production and commercialization [12,14–16]. One crucial task is process control for their eventual efficiency optimization. This task requires profound insights into the materials. Not only their morphologies, but also and particularly the processes taking place in them and their underlying mechanisms need to be taken into consideration.

On the basis of nature of molecules employed in organic photovoltaics, it might generally be classified into either small molecule solar cells (comprising small molecules) or polymer solar cells (containing giant molecules or polymers). Under this classification, various kinds of organic materials can be utilized in organic photovoltaics [17]. Polymer composites constitute another class of potential materials for OPV due to their low cost, environmental friendliness and capability of enhancing solar cell efficiency [18–20]. In the said context, Pinto and Maaroufi in a series of researches [21–23], suggested cheap and multipurpose bio-composites of urea-formaldehyde cellulose (UFC) filled with metal particles. These composite materials have shown quite interesting electrical/dielectric and thermal properties, particularly their considerably higher thermal stabilities [24,25]. However, irrelevant of the nature of organic materials used in an organic solar cell, the processes occurring in them under light exposure need to be studied particularly, as organic solar cells are generally known to demonstrate brisk degradation when illuminated [26]. Even more challenging task is the quantitative description of the mechanisms of photodegradation processes in OPVCs.

* Corresponding author.,
E-mail addresses: maaroufi@fsr.ac.ma, akarimmaaroufi@gmail.com (A. Maaroufi).

https://doi.org/10.1016/j.physb.2018.05.012
Received 26 February 2018; Received in revised form 7 May 2018; Accepted 9 May 2018
Available online 11 May 2018
0921-4526/

Photodegradation processes in materials occur due to their interactions with light. They may be categorized into several classes; though an important class of photodegradation processes which is of particular interest in the case of organic photovoltaics is the thermally accelerated photodegradation processes [27–33]. These processes are primarily initiated by light following a subsequent acceleration through temperature. Temperatures modulated UV/Vis or near infrared spectroscopic analyses are usually employed to investigate these processes by carrying out successive spectral scans of the reaction. The initial absorbance-wavelength spectrum usually corresponds to the light absorbing reactant and as the reaction advances, the total absorbance of process becomes the function of time and/or temperature. Thermally accelerated photodegradation processes can be modeled kinetically if the following criteria are satisfied.

- The determinancy of the influence of temperature on such processes is feasible.
- The rate limiting state is not too short lived to be determined.
- The thermal energy supplied to the reaction in the form of temperature is capable of accessing the activation energy barrier of reaction and not merely utilized in enhancing the collision frequencies of molecules participating in the reaction [34].
- The energy distribution along the relevant coordinates is governed by Boltzmann statistics.

Kinetic analysis of thermally accelerated photodegradation processes results in evaluating the activation parameters in order to analyze their transition states and eventually their process mechanisms [35]. The information obtained by kinetic study can be practically useful; for instance in predicting the stability/life of materials outside the experimental range which might be quite beneficial in the case of solar devices for renewable energy purposes [36–42]. It is however worth pointing out that despite the importance of kinetic analysis of thermally accelerated photodegradation processes, a systematic kinetic approach to kinetically interpret these processes has not yet been put forward in the literature. In this frame of reference, this paper rationally perceives the stated subject, and reports an advanced kinetic approach to simulate the reaction mechanisms of thermally accelerated photodegradation processes in organic photovoltaics. The efficacy of the proposed kinetic approach under isothermal/non-isothermal conditions and simple/complicated photodegradation processes will be justified. The validity conditions of the said kinetic approach along with some of its prospective applications on the organic photovoltaics will be discussed.

2. Theory of the kinetics of thermally accelerated photodegradation processes in organic photovoltaics

Fig. 1 demonstrates the basic diagram of an organic photovoltaic solar cell. In an organic photovoltaic cell, light is probably the most influential parameter regarding to the aging of principal photovoltaic conversion material i.e. photoactive layer. In general, light causes irreversible denaturing of photoactive layer of solar cell which shows acceleration with temperature. The extent of a thermally accelerated photodegradation process can be effectively described by a term degree of the advancement of reaction which is denoted by 'x' as given below [43]:

$$x = \frac{A_0 - A_t}{A_0 - A_\infty} \tag{1}$$

Where, 'A_0' is the initial absorbance of reactant, 'A_t' is reactant's absorbance at certain time/temperature, and 'A_∞' is its absorbance at the end of reaction. It is worth noting that the degree of advancement remains normalized within [0, 1] throughout the course of process.

In such processes, the reaction rate dx/dt being the function of 'x' can be described by the following expression:

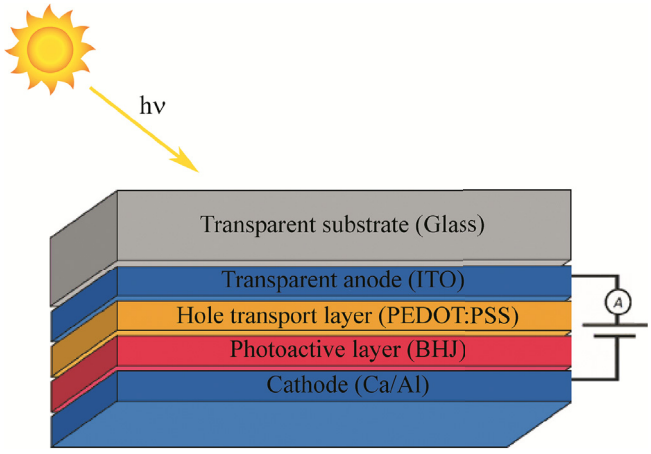

Fig. 1. Basic diagram of an organic photovoltaic solar cell.

$$\frac{dx}{dt} = kf(x) \tag{2}$$

Eq. (2) is the basic kinetic equation of thermally accelerated photoreaction processes including 'k' as the temperature dependent rate constant of reaction. The value of 'k' might be appropriately substituted in Eq. (2) by Arrhenius equation which then takes the following form:

$$\frac{dx}{dt} = Z\exp(-E/RT)f(x) \tag{3}$$

In Eq. (3), Z is the pre-exponential factor, E is the energy of activation and $f(x)$ is a function of degree of the advancement of reaction, called reaction model. Physically, Z describes the collision frequency of particles involved in the formation of activated complex, E is the energy barrier of reaction, and $f(x)$ is the mechanistic function which is capable of providing information about the mechanism of process, also called reaction model [44].

The dependence of the degree of advancement of a thermally accelerated photodegradation process and its activation parameters may be expressed by the following general scheme:

$$x = \Phi_1(T, t);\ E = \Phi_2(x, T);\ Z = \Phi_3(x, T)$$

It should be noticed that the photo-activation of photodegradation processes might depend on the wavelength of incident light [45]. In order to illustrate this, the work of H. Hintz et al. is taken into account, as detailed in Ref. [31]. H. Hintz et al. carried out a quantitative analysis of the influence of environmental factors including, variation of intensity and spectral distribution of the incident light, oxygen concentration, humidity level as well as temperature on the degradation process of poly(3-hexyl thiophene) (P3HT) film.

The authors pointed out wavelength dependence of photodegradation of P3HT films (Fig. 2) and gave a rational description of the phenomenon. In their accordance, P3HT (regio-regular) isomer presents a strongly structured absorption spectrum in the solid state with the vibronic bands located at roughly 520 nm, 554 nm and 610 nm. Both the vibronic bands at 554 nm and 610 nm are strongly affected by interchain interactions, which in turn depend on the crystallinity of the polymer film. As a matter of fact, the absolute absorption maximum is observed at 520 nm in more amorphous films, while it is available at 554 nm in relatively more crystalline films [31]. Photodegradation mechanisms of P3HT films could differ at different maxima of wavelength-absorbance spectrum (Fig. 2) due more likely to different kinetics. Taking into consideration the mentioned case, it is highly probable in wavelength-absorbance spectra of a polymer solar material film that each of the maxima may correspond to a certain mechanism contributing to the whole degradation process. Evaluation of thermally accelerated photodegradation kinetics and modeling reaction mechanism at variable wavelength thus becomes highly complicated.

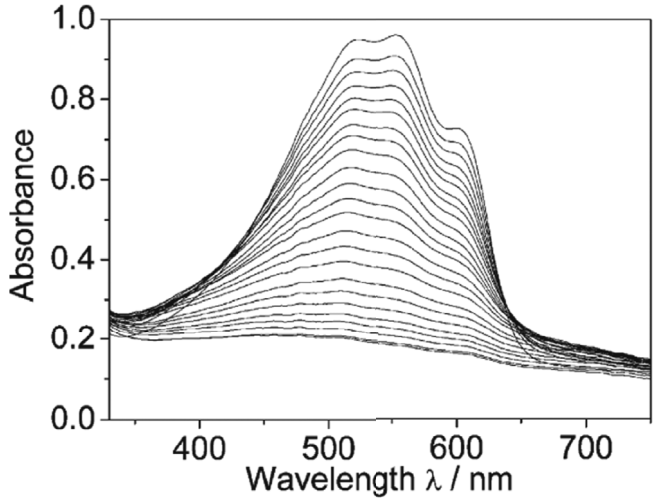

Fig. 2. UV/Vis spectra of regioregular P3HT thin films during photo-oxidation [31] (reused with kind permission from American Chemical Society).

Therefore, the variation in x with time and/or temperature (Eq. (3)) is measured at a certain wavelength (preferably, wavelength corresponding to maximum absorbance). Although, the kinetic modeling of such processes at different wavelengths could allow estimating the probable variation in the pathways of these reactions and to fairly predict more complicated photodegradation mechanisms under variable wavelengths.

The pre-exponential factor is known to vary with temperature by following the relationship as given below:

$$\frac{Z}{Z_0} = \left(\frac{T}{T_0}\right)^m \tag{4}$$

Where as, 'Z_0' is the value of pre-exponential factor at initial temperature 'T_0' (usually room temperature) and 'm' is a numerical constant. Usually, $m \in [0, 1]$ but it may have positive values other than mentioned in the interval and it can even be a negative number. Comparison of Eq. (4) with the theoretical expression of transition state theory sheds light on the probable physical significance of the parameter m. In fact, the parameter m in Eq. (4) can be helpful in extracting rather detailed mechanistic information complementary to the reaction model [46].

Substitution of the value of Z from Eq. (4) into Eq. (3) yields the following equation:

$$\frac{dx}{dt} = Z_0 (T/T_0)^m \exp(-E/RT) f(x) \tag{5}$$

Equation (5) can be considered as a generalized kinetic equation to analyze the thermally accelerated photodegradation processes in organic photovoltaics. Some of the well known condense phase reaction model expressions in Eq. (5) are shown in Table 1 and Fig. 3a.

3. Derivation of activation energies and mechanistic functions of thermally accelerated photodegradation processes

3.1. Determination of activation energy

Determination of activation energy is an initial step towards the evaluation of mechanistic function or reaction model, necessary for mechanistic predictions. For this purpose, a systematic determination of the activation energies of photodegradation process under consideration is carried out. The systematic determination of activation energy is credible because:

- Activation energy determined by taking into account different thermal histories reveals simple or complex nature of process. A process may fairly be approximated as single-step if the variation in its activation energy with the degree of reaction advancement is insubstantial, otherwise, the reaction is perceived as following a complex reaction pathway [47–50].
- Different reaction models might fit a single kinetic dataset by accomplishing mutual compensation between pre-exponential factors and activation energies [47,50]. The true kinetic triplet i.e. a combination of Z, E and f(x) in that case is entirely obscure.

Taking into consideration the above arguments, Eq. (5) can be rearranged into the following expression:

$$\frac{dx}{dt} = Z_0 f(x)(T/T_0)^m \exp(-E/RT) \tag{6}$$

Where, Z_0 remains independent of the degree of the advancement of reaction during the reaction course [39]. Under invariant conditions of x, Eq. (6) is transformed into the following equation:

$$w = a(y/const.)^b \exp(-c/y) \tag{7}$$

Where, y = T; w = dx/dt; a = φ(x) = Z_0f(x); b = m; c = E/R and const. = T_0

Equation (7) provides basis for a non-linear differential method to determine the activation energies of photodegradation processes. The variation in reaction rate with temperature at a number of constant values of x belonging to [0, 1] under either isothermal or non-isothermal conditions can be fitted using non-linear regression which results in the generation of required parameters a, b and c [24,46].

3.2. Evaluation of reaction models of photodegradation processes

3.2.1. Reaction models in the case of non-isothermal photodegradation processes

In order to determine the reaction models of photodegradation processes taking place in organic photovoltaics under non-isothermal conditions, Eq. (6) can be rearranged after taking its logarithm as following:

$$\ln\left(\frac{dx}{dt}\right) = \ln Z_0 + m(\ln T - \ln T_0) - E/RT + \ln f(x) \tag{8}$$

The overall change in the reaction rate with respect to degree of advancement of reaction 'x' as process goes forward under non-isothermal conditions can be described by differentiating Eq. (8) with respect to 'x' as following:

$$\frac{1}{dx/dt}\frac{d}{dx}\left(\frac{dx}{dt}\right) = \frac{m}{T}\frac{dT}{dx} - \left\{\frac{TdE/dx - EdT/dx}{RT^2}\right\} + \frac{f'(x)}{f(x)} \tag{9}$$

Using chain rule of differentiation, $d/dx(dx/dt) = d/dt(dx/dt)(dt/dx) = (d^2x/dt^2)/(dx/dt)$, and also, $dT/dx = 1/(dx/dT) = \gamma/(dx/dt)$. Where, $\gamma = dT/dt$, is the heating rate. Rearranging Eq. (9) gives,

$$\frac{d^2x/dt^2}{(dx/dt)^2} = \frac{\gamma m}{Tdx/dt} - \frac{dE/dx}{RT} + \frac{\gamma E}{RT^2 dx/dt} + \frac{f'(x)}{f(x)} \tag{10}$$

Rearrangement of Eq. (10) gives,

$$\frac{f'(x)}{f(x)} = \frac{dE/dx}{RT} - \frac{\gamma}{Tdx/dt}\left\{m + \frac{E}{RT}\right\} + \frac{d^2x/dt^2}{(dx/dt)^2} \tag{11}$$

Using chain rule of differentiation, $dE/dx = (dE/dT)(dT/dx) = \gamma(dE/dT)/(dx/dt)$, Eq. (11) takes the following form:

$$\frac{f'(x)}{f(x)} = \frac{\gamma}{dx/dt}\left[\frac{dE/dT}{RT} - \frac{1}{T}\left\{m + \frac{E}{RT}\right\} + \frac{d^2x/dt^2}{\gamma dx/dt}\right] \tag{12}$$

Both Eqs. (11)-(12) deal with the determination of reaction models of thermally accelerated photodegradation processes under non-isothermal conditions. By definition, Eqs. (11)-(12) should provide similar

Table 1
Well known condensed phase reaction models with their respective *g(x)* expressions.

Reaction model	Notation	*f(x)*	*g(x)*
Reaction order	*RO (n)*	$(1- x)^n$	$^{-n/(1-x)}$
Jhonson Mehl Avrami general equation	*JMA(p)*	$p(1-x)\{-\ln(1-x)\}^{1-1/p}$	$-\frac{\left\{1+\frac{1-1/p}{\ln(1-x)}\right\}}{1-\alpha}$
1D diffusion	*D1*	$1/2x$	$-1/x$
2D diffusion	*D2*	$-1/\ln(1\text{-}x)$	$1/\ln(1\text{-}x)^{1\text{-}x}$
3D diffusion (Jander's equation)	*D3*	$\frac{3(1-x)^{2/3}}{2\{1-(1-x)^{1/3}\}}$	$-\frac{2}{3}\left[\frac{1}{1-x}+\frac{1}{2(1-x)^{2/3}\{1-(1-x)^{1/3}\}}\right]$
3D diffusion (Ginstling equation)	*D4*	$\frac{3}{2\{(1-x)^{-1/3}-1\}}$	$-\frac{1}{3}\left[\frac{1}{\{(1-x)^{-1/3}-1\}(1-x)^{4/3}}\right]$
Šesták-Berggren	*SB (m, n)*	$(x)^m(1\text{-}x)^n$	$\frac{m}{x}-\frac{n}{1-x}$
Power law	Pr	$r(x)(1-1/r)$	$\frac{\left(1-\frac{1}{r}\right)}{x}$

results ignoring the numerical differentiation error.

In the case of single-step photodegradation processes, *dE/dx* and *dE/dT* tend to zero and therefore, Eqs. (11)-(12) take the following form:

$$\frac{f'(x)}{f(x)}=\frac{d^2x/dt^2}{(dx/dt)^2}-\frac{\gamma}{Tdx/dt}\left\{m+\frac{E}{RT}\right\} \tag{13}$$

3.2.2. Reaction models in the case of isothermal photodegradation processes

In isothermal kinetic analysis of photodegradation processes, temperature is kept constant. Therefore, putting $\gamma = 0$ *in* Eq. (11) and rearranging it yields:

$$\frac{f'(x)}{f(x)}=\frac{dE/dx}{RT}+\frac{d^2x/dt^2}{(dx/dt)^2} \tag{14}$$

Equation (14) takes the following form if the reaction consists of only one step:

$$\frac{f'(x)}{f(x)}=\frac{d^2x/dt^2}{(dx/dt)^2} \tag{15}$$

Equation (15) points out that if a photodegradation process follows single-step isothermal kinetics then its reaction mechanism can be directly evaluated without the information of its activation energy and pre-exponential factor.

Aiming at determining the mechanistic functions of photodegradation processes, the ratio between differentiated and actual reaction models described in Eqs. 11–15, can be expressed as a function *g(x)* as shown below:,

$$g(x)=\frac{f'(x)}{f(x)} \tag{16}$$

The right hand sides of Eqs. 11–15 can either be calculated by simulated kinetic data (numerical analysis/simulation) or experimental kinetic data (practical data) while the left hand sides may be modeled by the *g(x)* expressions of the most common reaction models, as shown in Table 1 and Fig. 3b. A fair correlation between the simulated/experimental and theoretical curves (Fig. 3b) guides to the most probable reaction model and therefore the mechanism. Nevertheless, it has been pointed out that the *g(x)* function is appropriate in the case of single-step reactions and multi-step reactions may provide intricate shapes of *g (x)* function [50]. Following the same conception, the reaction models of complicated photodegradation processes may be estimated by

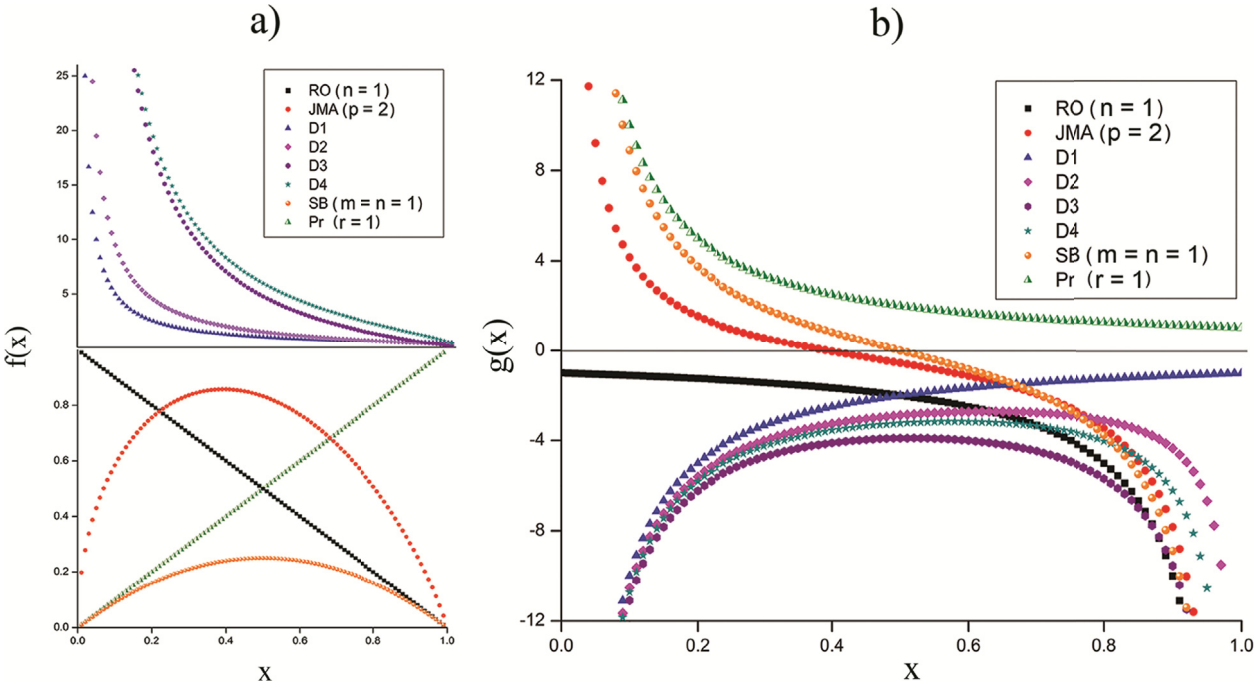

Fig. 3. (a) Graphical expressions of well known condense phase reaction models with reference to Table 1. (b) *g(x)* plots of the respective reaction models.

integrating Eq. (16) as following:

$$f(x) = \exp\left(\int_{x_0}^{1} g(x)dx\right) \tag{17}$$

Where, x_0 is a value greater than zero obtained by the addition of an infinitesimally small positive digit to zero. The reaction models of photodegradation processes can be calculated by performing numerical integration of the curve obtained from Eqs. (11)-(12) for non-isothermal kinetics and Eq. (14) for isothermal kinetics over (0, 1]. A suitable numerical integration algorithm which is recommended here is the modified Guassian Quadrature [51]. In addition, it is worth mentioning that the suggested kinetic methods are based upon a purely differential approach which inevitably demands numerical differentiation and therefore, care must be taken to compute the precise values of reaction model(s). The noise in numerical data of dE/dx, dE/dT and d^2x/dt^2 may be significantly reduced by determining them in an infinitesimal interval of 'x' say, $[x,\ x+\Delta x]_{\Delta x\to 0}$ and using well known Savitzky–Golay's smoothing filter.

A critical issue in the case of overlapping complex multi-step processes is associated with identifying the mechanisms of the individual reactions within them. This trouble originates from the fact that only nucleation/growth models show peak functions, and the rest of reaction models (if available) might not be visible in the plots of $f(x)$, as evident in Fig. 3a. In order to solve this matter, a kinetic function $F(x, T)$, taking into account the variation of reaction mechanism with temperature, is suggested in non-isothermal kinetics which can be defined as:

$$F(x,\ T) = \frac{df(x)}{dT} = f'(x)\frac{dx}{dT} = \frac{1}{\gamma}f'(x)\frac{dx}{dt} \tag{18}$$

The obtained characteristic shapes of $F(x, T)$ functions by applying Eq. (18) on the reaction models shown in Fig. 3a, using an arbitrary single-step reaction simulated by Runge-Kutta (RK4) method at $\gamma = 10\ ^{\circ}\text{C.min}^{-1}$, are represented in Fig. 4.

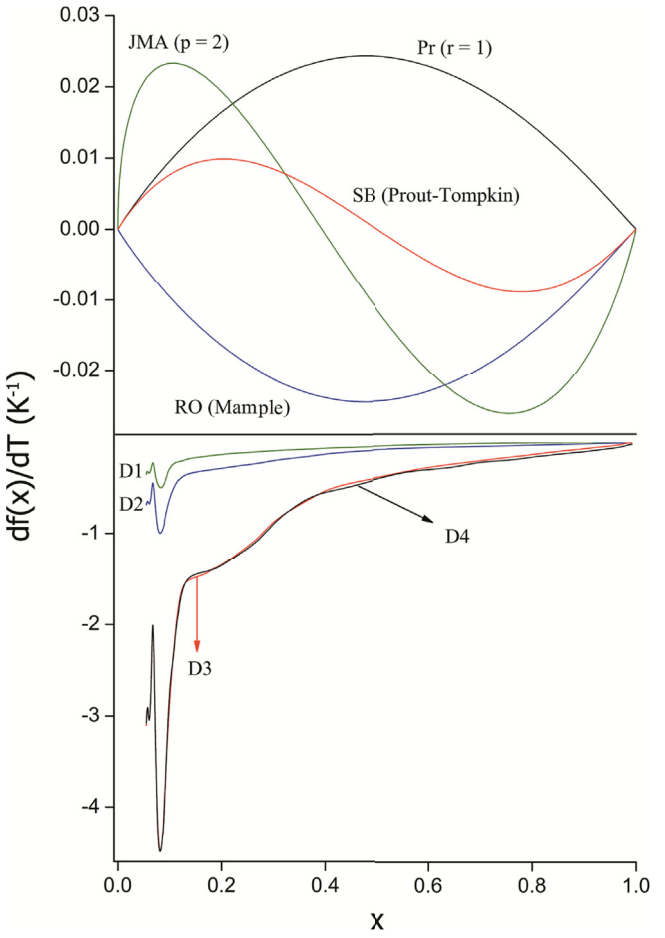

Fig. 4. Graphical representation of the application of $F(x, T)$ function on the reaction models shown in Fig. 3a, at $\gamma = 10\ ^{\circ}\text{C.min}^{-1}$ heating rate.

4. Generation of kinetic data

In order to trial the applicability and effectiveness of the suggested kinetic approach, kinetic data are generated by taking into account simulated thermally accelerated photodegradation processes in OPVCs, employing numerical analysis. It is noteworthy that the selection of kinetic triplets and associated parameters in simulated processes is purely arbitrary.

4.1. Single-step photodegradation process

4.1.1. Isothermal case

The reaction rate of a second order isothermal reaction is simulated by employing Eq. (5) at different isothermal runs at; $T \in [70,\ 100]$ with temperature difference of 10 °C. The utilized initial temperature, activation parameters and numerical constant 'm' have been; $T_0 = 25\ ^{\circ}\text{C}$, $Ea = 100\ \text{kJ mol}^{-1}$, $Z_0 = 10^{13}\ \text{min}^{-1}$ and $m = 1$. At each isothermal run, the x-t plots are drawn by numerically integrating the dx/dt against x curves. The results obtained are shown in Fig. 5a.

4.1.2. Non-isothermal case

The single-step non-isothermal photocrystallization following 2D continuous nucleation ($p = 2$) at different heating rates; $\gamma = 5$, 10, 15, 20 °C/min is simulated by approximating ordinary differential Eq. (19) which is derived by modifying Eq. (5), taking into account Johnson-Mehl-Avrami model (Table 1).

$$\frac{dx}{dT} = \frac{pZ_0}{\gamma}(T/T_0)^m \exp(-E/RT)(1-x)\{-\ln(1-x)\}^{1-1/p} \tag{19}$$

The method used to numerically solve Eq. (5) in order to obtain x-T curves at each heating rate is 4th order Runge-Kutta method (RK4). The employed initial temperature, activation parameters and numerical constant 'm' have been; $T_0 = 25\ ^{\circ}\text{C}$, $Ea = 100\ \text{kJ mol}^{-1}$, $Z_0 = 10^{11}\ \text{min}^{-1}$ and $m = 1$. At each non-isothermal history, the reaction rate is calculated by numerically differentiating the x-T curve. The obtained results are shown in Fig. 5b.

4.2. Multi-step photodegradation process

4.2.1. Parallel reactions under isothermal conditions

The following kinetic equation of two independent parallel first order reactions is taken into consideration in this case:

$$\frac{dx}{dt} = (Z_0)_1(T/T_0)^{m_1}\exp(-E_1/RT)(1-x_1)^{n_1} + (Z_0)_2(T/T_0)^{m_2}\exp(-E_2/RT)(1-x_2)^{n_2} \tag{20}$$

It is assumed that both the reactions equally contribute in the whole process. The overall reaction rate is simulated by Eq. (20) at different temperatures; $T \in [70,\ 100]$ with temperature difference of 10 °C. The employed initial temperature, activation parameters, and numerical constants are; $T_0 = 25\ ^{\circ}\text{C}$, $E_1 = 70\ \text{kJ mol}^{-1}$, $E_2 = 90\ \text{kJ mol}^{-1}$, $(Z_0)_1 = 10^9\ \text{min}^{-1}$, $(Z_0)_2 = 10^{12}\ \text{min}^{-1}$and $m_1 = m_2 = 1$. At each isothermal run, the x-t plots are drawn by numerically integrating the dx/dt versus x curves and the obtained results are shown in Fig. 5c.

4.2.2. Consecutive reactions under non-isothermal conditions

Multi-step nucleation/growth mechanism is simulated by taking into account three different reactions occurring consecutively by following Johnson-Mehl-Avrami model with $p_1 = 2$; $p_2 = 4$ and $p_3 = 1/2$, respectively. The individual reactions have been simulated by Eq. (19)

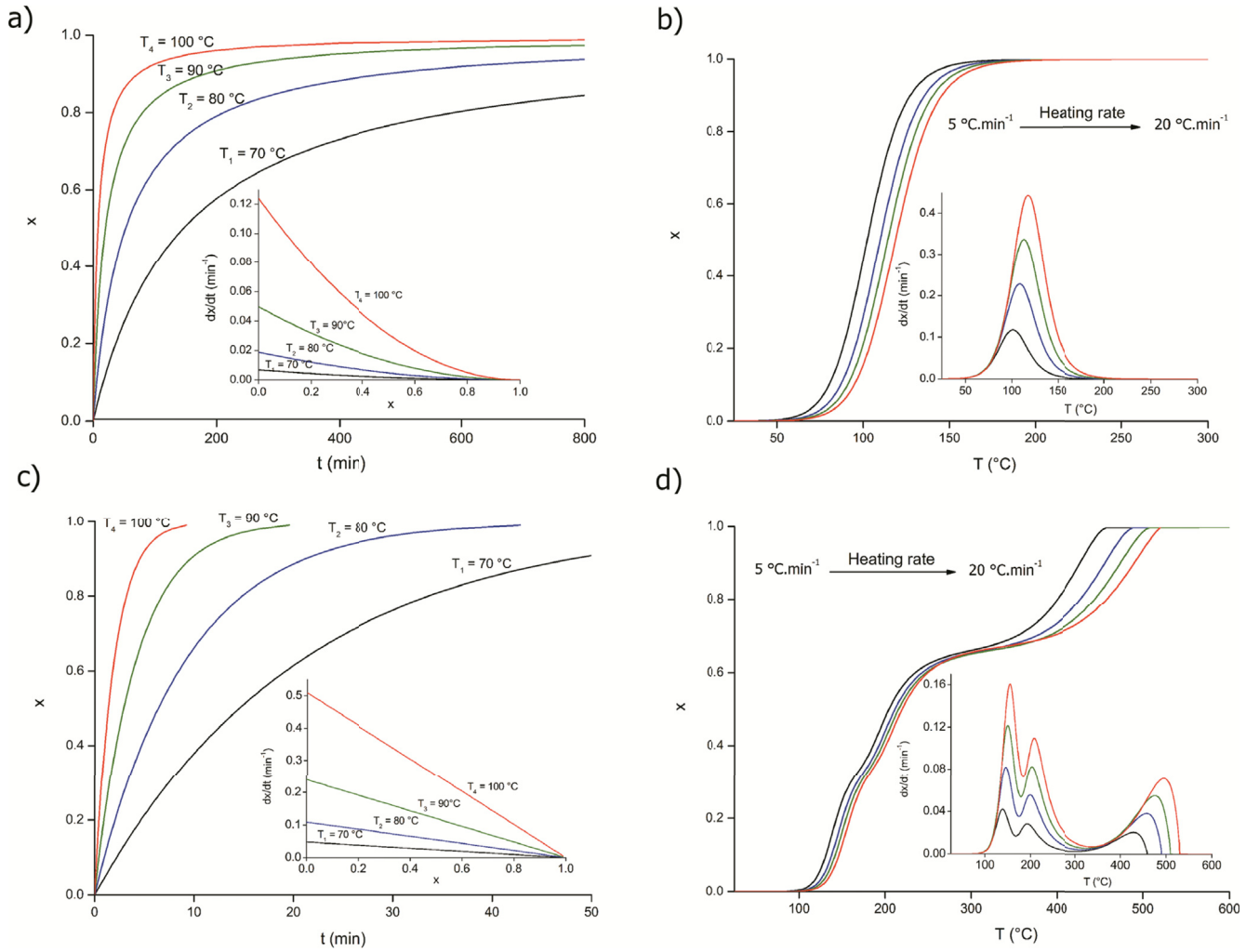

Fig. 5. Generation of simulated data. (a) Single-step isothermal photodegradation process; inset: reaction rate. (b) single-step non-isothermal photocrystallization process; inset: reaction rate. (c) Multi-step parallel isothermal photodegradation processes; inset: reaction rate. (d) Multi- step consecutive non-isothermal photodegradation processes; inset: reaction rate.

following the procedure already discussed in one of the previous sections and afterwards a partially overlapping convoluted multi-step reaction profile at each heating rate is developed by taking equal contributions of the reactions participating in photodegradation. The employed initial temperature, activation parameters and numerical constants of all the reactions are: $T_0 = 25\,^{\circ}C$, $E_1 = 130\,kJ\,mol^{-1}$, $E_2 = 175\,kJ\,mol^{-1}$, $E_3 = 85\,kJ\,mol^{-1}$; $(Z_0)_1 = 10^{16}$ min^{-1}, $(Z_0)_2 = 10^{19}$ min^{-1} $(Z_0)_3 = 10^5$ min^{-1} and $m_1 = m_2 = m_3 = 1$. The obtained results are shown in Fig. 5d.

5. Results and discussion

5.1. Determination of activation energies and their interpretations

In order to determine the activation energies, non-linear differential method as expressed in Eq. (7) is employed on the kinetic data of simulated photodegradation process. As the reaction rates of thermally accelerated photodegradation processes vary exponentially with temperature, the variation in reaction rate with temperature at a certain set of constant values of x can be fitted by a user defined fitting function (UDF) based on Eq. (7) employing Levenberg-Marquardt algorithm (LMA) for 2D curves [35], which results in the required parameters a, b and c. Fig. 6a–d shows the application of non-linear differential method on simulated data in the case of isothermal and non-isothermal, and simple and complicated thermally accelerated photodegradation processes. The results obtained by employing non-linear differential method on the kinetic data of simulated processes are shown in Fig. 7a–d, including correlation factors and error bars in each case.

Figs. 5a and 6a show the results obtained by applying non-linear differential method on the kinetic data of simulated single-step isothermal photodegradation process as already demonstrated graphically in Fig. 5a. The insignificant variation in activation energy with the degree of reaction advancement in Fig. 7a verifies the single step nature of reaction. The activation energy has been found $97 \pm 4\,kJ\,mol^{-1}$, which is in good agreement with the activation energy used to generate the simulated data. Similarly, Figs. 5b and 6b depict the results generated by the application of non-linear differential method on the kinetic data of simulated single-step non-isothermal photocrystallization as demonstrated in Fig. 5b. Insubstantial variation in activation energy with respect to degree of the advancement of reaction in Fig. 7b verifies the single-step nature of reaction. The activation energy in this case has been found $95 \pm 5\,kJ\,mol^{-1}$, which is in good agreement with the value used to generate the simulated data.

Figs. 5c and 6c represent the results obtained by employing non-linear differential method on the kinetic data of simulated multi-step competitive isothermal photodegradation process as demonstrated in Fig. 5c. It is worth noticing in Fig. 7c that the activation energy barriers of both the photodegradation processes overlap to generate a single activation energy barrier with an average energy of $81 \pm 7\,kJ\,mol^{-1}$. This phenomenon also unravels the complexity underlying in kinetic

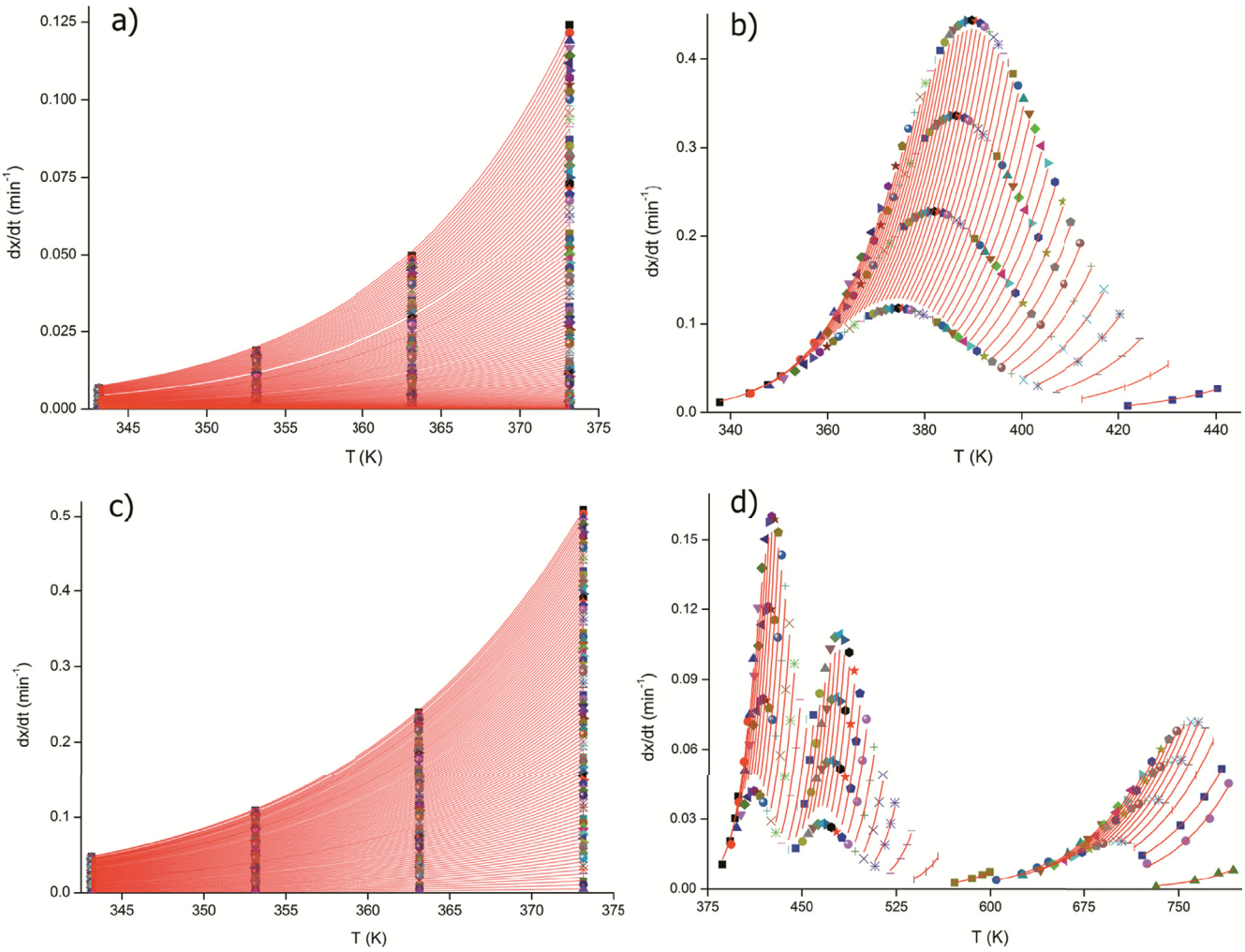

Fig. 6. Application of non-linear differential method on (a) Single-step isothermal process. (b) Single-step non-isothermal process. (c) Multi-step isothermal process. (d) Multi-step non-isothermal process.

modeling of parallel reactions.

Figs. 5d and 6d show the results obtained by applying non-linear differential method on the kinetic data of simulated multi-step consecutive photodegradation process under non-isothermal conditions. The variation in activation energy with the advancement of reaction in Fig. 7d verifies that the reaction goes to completion by following three fairly separable steps, verifying its consecutive nature. The first step ranges around 30% of conversion with average activation energy of $137 \pm 5\,\mathrm{kJ\,mol^{-1}}$. The second step ranges around 65% of conversion with average activation energy of $178 \pm 6\,\mathrm{kJ\,mol^{-1}}$. The third and the last step has average energy of $90 \pm 3\,\mathrm{kJ\,mol^{-1}}$. These average energies are in good agreement with the activation energies used to generate the simulated data. The correlation factor and the numerical constant in each case attain an approximate value unity, as can be observed in Fig. 7a–d.

5.2. Determination of reaction models and mechanistic predictions

In order to predict the most probable reaction mechanisms of thermally accelerated photodegradation processes, methodology developed in the theoretical section is applied on the kinetic data of simulated processes. Results obtained by the application of Eq. (15) on the kinetic data of simulated isothermal single-step photodegradation process as already demonstrated graphically in Fig. 5a, are shown in Fig. 8a.

Comparison of the *g(x)* function in the inset of Fig. 8a with Fig. 3b suggests reaction order model for the reaction taken under consideration. The *g(x)* function in the inset of Fig. 8a is also fitted well by RO (n) model with $n = 2$, proposing a second order photodegradation process. Similarly, the results obtained by the application of Eq. (13) on the kinetic data of non-isothermal single-step photocrystallization as demonstrated in Fig. 5b are inserted in Fig. 8b. *g(x)* function in the inset of Fig. 8b elucidates that reaction follows nucleation/growth mechanism which is fairly fitted by *g(x)* function of JMA model, generating $p = 1.91$. This information is in fair agreement with that used to generate the simulated kinetic data of single-step non-isothermal photocrystallization following 2D continuous nucleation.

In the third case the application of non-linear differential method on the kinetic data of multi-step isothermal processes has generated effective activation energy of $81 \pm 7\,\mathrm{kJ\,mol^{-1}}$ as discussed in the previous section. In order to verify whether reaction follows a single-step or a multi-step pathway, *φ(x)* function deduced from non-linear differential method versus degree of conversion is shown in Fig. 8c.

The shape of *φ(x)* function elucidates the reaction complexity. Therefore, Eq. (14) is employed on the relevant kinetic data, and the obtained results are represented in Fig. 8c. The shape of *g(x)* function in the inset of Fig. 8c does not correspond to the *g(x)* graph of any of the known reaction models, pointing out its complex pathway. The shape of reaction model in this case has been drawn by employing Eq. (17) which conforms to the shape of *φ(x)* function. Although, by the minor variation of activation energy with the degree of reaction advancement in Fig. 8c and the appearance of maximum reaction rate at more or less

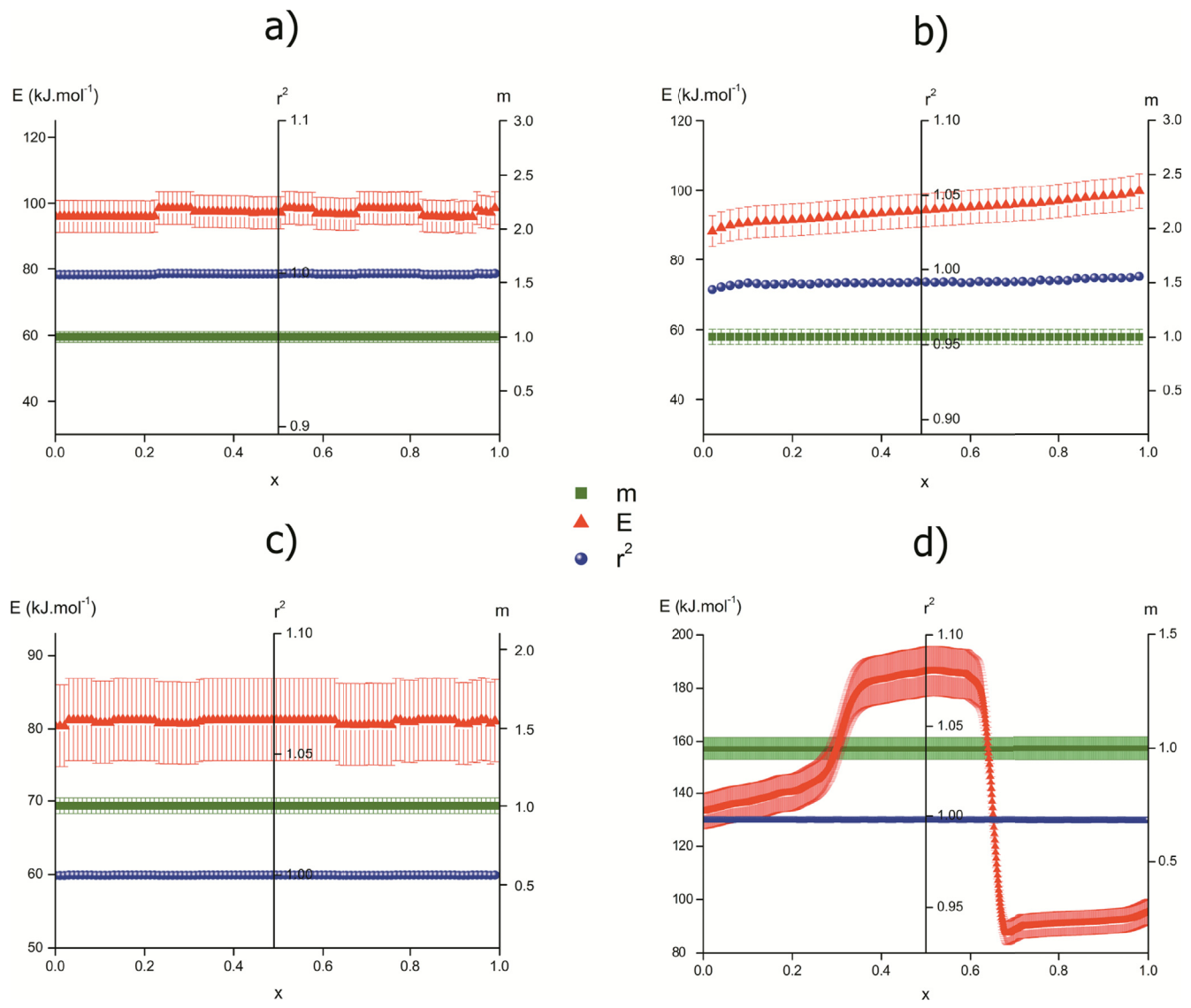

Fig. 7. Activation energy *E* and numerical constant *m* along with the relevant correlation factors obtained by applying non-linear differential method on (a) Single-step isothermal process. (b) Single-step non-isothermal process. (c) Multi-step isothermal process. (d) Multi-step non-isothermal process.

the reaction startup, the process could be mistaken as single-step following reaction order model, yet *g(x)* and *f(x)* function show that it is composed mainly of at least two reactions. The information obtained from Figs. 6c, 7c and 8c suggest that the most probable mechanism followed by the process is the overlapping parallel first order reactions. In the similar way, Fig. 8d is drawn by applying Eq. (11) on the kinetic datasets of simulated non-isothermal mutli-step photodegradation process as demonstrated in Fig. 5d. The shape of *g(x)* function in the inset of Fig. 8d confirms the complexity of photodegradation process, and the shape of *f(x)* shows that the process apparently advances by following three overlapping nucleation/growth phenomena.

In order to determine the nature of each contributing process in the overall photodegradation process in the forth case, Eq. (18) is employed on the relevant kinetic data. The obtained results are shown in Fig. 9a. The plot of reaction model in Fig. 9a can be divided into three different regions. Although apparently the three process seem to follow nucleation/growth phenomena, yet it is evident from the plot of variation in reaction model with temperature that the mechanism in third region is quite different from the rest of the two as can be observed by making a comparison of *df(x)/dT* plot in Fig. 9a with the *df(x)/dT* plots of well known reaction models in Fig. 4. As a matter of fact, it has been recently reported that the JMA model is not merely restricted to nucleation/growth but relatively higher values of JMA model parameter within (0, 1) might be attributed to the complex diffusion processes occurring in solid state [52]. The resemblance in the behavior shown by *df(x)/dT* plots of JMA ($p = 0.5$), used to generate the simulated data, and Jander's diffusion model in Fig. 9b verifies that finding.

It is also worth paying attention that the concept of *F(x, T)* function seems practically better than the peak deconvolution of multi-step reaction models because the latter may ends up with unreliable results and hence unreasonable mechanistic information.

6. Conclusion

- The prominent advantages of the suggested kinetic approach to predict the mechanisms of photodegradation processes include its equal contribution in isothermal as well as non-isothermal photodegradation kinetics, and covering single-step/multi-step processes. On the basis of the developed kinetic methods, probable pathways of complex photodegradation processes might be plausibly proposed.
- The function of variation in reaction model with temperature can be quite useful in distinguishing between the individual processes in multi-step non-isothermal photodegradation processes and subsequently identifying their mechanisms.

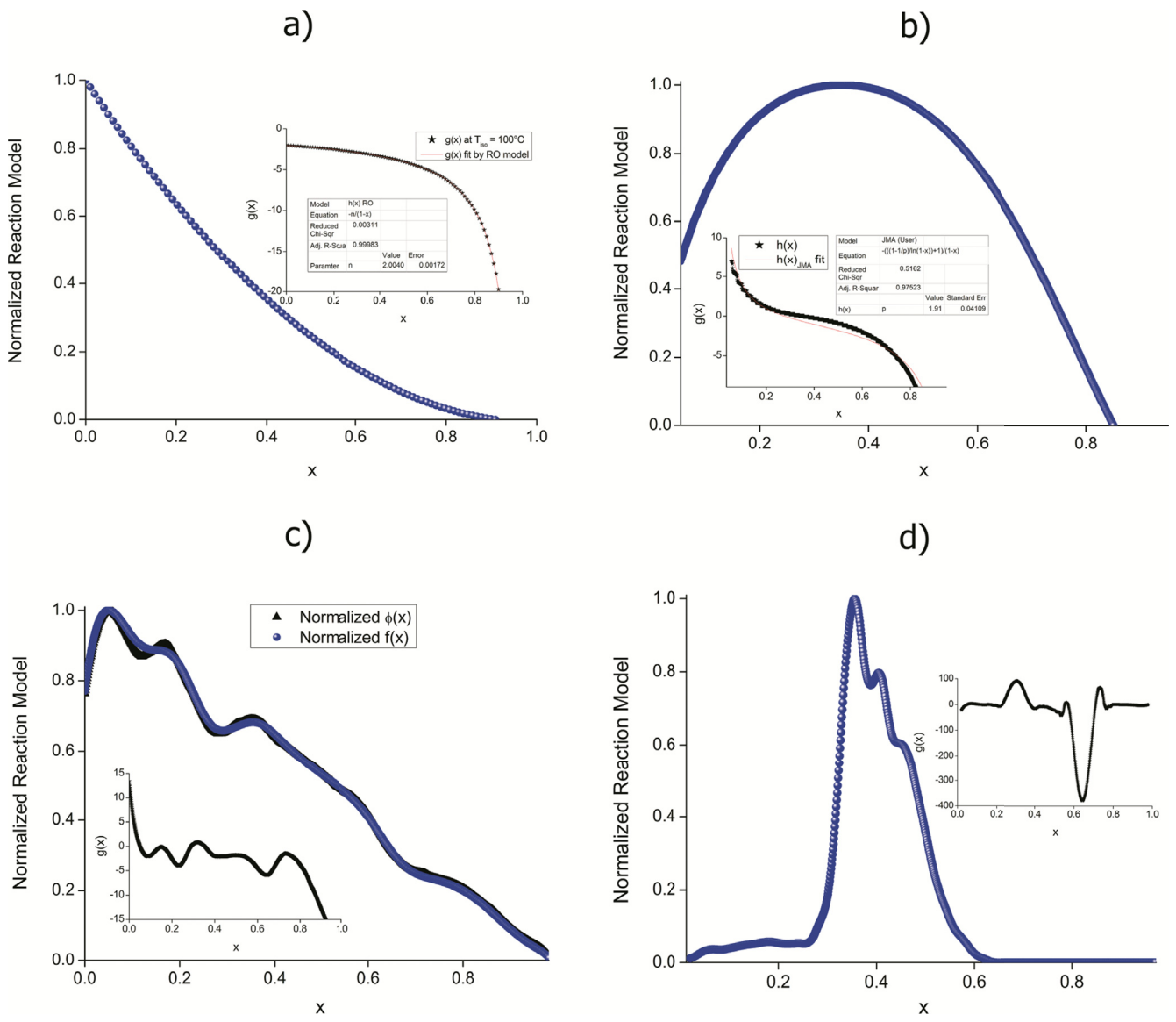

Fig. 8. Evaluation of reaction model *f(x)* by the suggested kinetic approach in the case of (a) Single-step isothermal process at 100 °C; inset: *g(x)* expression. (b) Single-step non-isothermal process; inset: *g(x)* expression at $\gamma = 10\ ^{\circ}C.min^{-1}$. (c) Multi-step isothermal process; inset: *g(x)* expression at 100 °C and its comparison with relative reaction model *φ(x)*, d) Multi-step non-isothermal process; inset: *g(x)* expression, at $\gamma = 10\ ^{\circ}C.min^{-1}$.

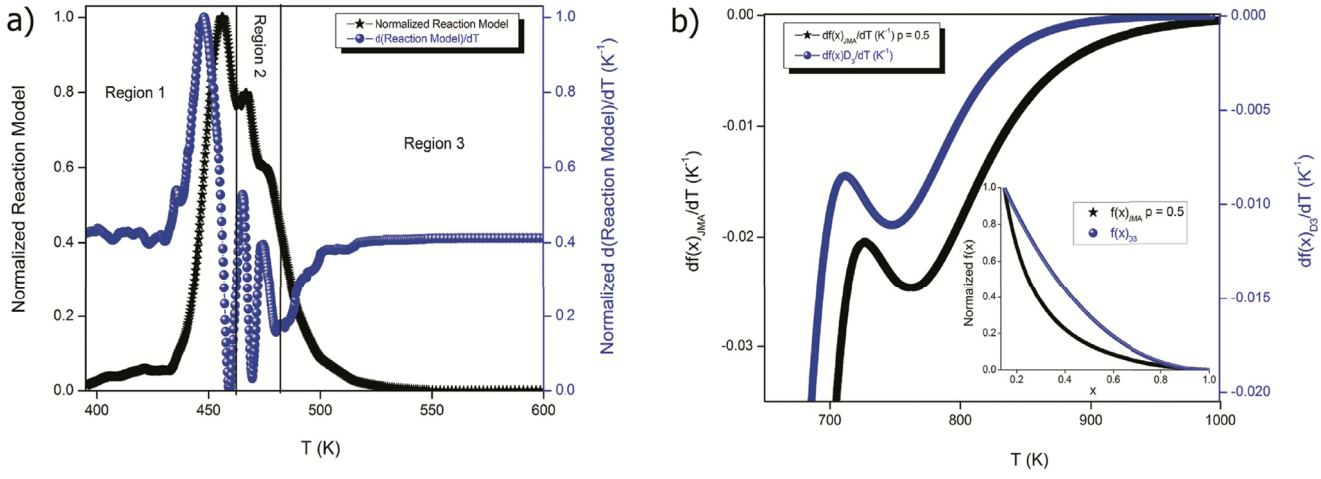

Fig. 9. a) Application of *F(x, T)* function on the multi-step non-isothermal consecutive photodegradation processes. (b) Comparison between $df(x)_{JMA}/dT$ versus *T* ($p = 0.5$) and $df(x)_{D3}/dT$ versus T while, D3 = Jander's diffusion model; inset: $f(x)_{JMA}$ ($p = 0.5$) and $f(x)_{D3}$.

- Overall, the suggested kinetic approach rationally responds to certain critical challenges being faced by the organic photovoltaics today. This research could potentially provide basis to eventual commercialization of the organic photovoltaic devices.

Conflicts of interest

The authors declare no conflict of interest.

Compliance with ethics requirements

It is declared that this article is in entire compliance with the research ethics.

Appendix A. Supplementary data

Supplementary data related to this article can be found at https://doi.org/10.1016/j.physb.2018.05.012.

References

[1] N. Asim, K. Sopian, S. Ahmadi, et al., Renew. Sustain. Energy Rev. 16 (2012) 5834–5847.
[2] A.J. Moule, Curr. Opin. Solid State Mater. Sci. 14 (2010) 123–130.
[3] http://www.cop21paris.org/about/cop21, last retrieved on May, 7, 2018.
[4] Y. Sun, W. Zhang, H. Chi, et al., Renew. Sustain. Energy Rev. 43 (2015) 973–980.
[5] J.-S. Cho, S. Baek, S. Park, et al., Sol. Energy Mater. Sol. Cells 102 (2012) 50–57.
[6] K.H. Solangi, M.R. Islam, R. Saidur, et al., Renew. Sustain. Energy Rev. 15 (2011) 2149–2163.
[7] S. Holliday, S. Li, C.K. Luscombe, Prog. Polym. Sci. 70 (2017) 34–51.
[8] G. Han, S. Zhang, P.P. Boix, et al., Prog. Mater. Sci. 87 (2017) 246–291.
[9] L. Hu, F. Wu, C. Li, et al., Macromolecules 48 (2015) 5578–5586.
[10] F. Meyer, Prog. Polym. Sci. 47 (2015) 70–91.
[11] C.E. Small, S.-W. Tsang, S. Chen, et al., Adv. Energy Mater. 3 (2013) 909–916.
[12] P. Kumar, S. Chand, Prog. Photovolt. Res. Appl. 20 (2012) 377–415.
[13] Y. Yongbo, J.R. Timothy, S. Pankaj, et al., Nat. Mater. 10 (2011) 296–302.
[14] A. Polman, M. Knight, E.C. Garnett, et al., Science 352 (2016) 1–10.
[15] M.Y. Ameen, P. Shamjid, T. Abhijith, et al., Physica B 530 (2018) 201–207.
[16] Special Issue Entitled: “Degradation and stability of polymer and organic solar cells”, in: F.C. Krebs (Ed.), Sol. Energy Mater. Sol. Cells 92 (2008) 685–820.
[17] J. Nelson, Mater. Today 14 (2011) 462–470.
[18] G. Keru, P.G. Ndungu, V.O. Nyamori, Int. J. Energy Res. 38 (2014) 1635–1653.
[19] Y. Sun, G. Shi, J. Polym. Sci. B Polym. Phys. 51 (2013) 231–253.
[20] D. Angmo, F.C. Krebs, J. Appl. Polym. Sci. 129 (2013) 1–14.
[21] G. Pinto, A. Maaroufi, Polym. Compos. 26 (2005) 401–406.
[22] G. Pinto, A. Maaroufi, J. Appl. Polym. Sci. 96 (2005) 2011–2015.
[23] G. Pinto, A. Maaroufi, Polym. Compos. 33 (2012) 2188–2194.
[24] M.A. Arshad, A. Maaroufi, Rev. Adv. Mater. Sci. 51 (2017) 177–187.
[25] M.A. Arshad, A. Maaroufi, R. Benavente, G. Pinto, J. Mater. Sci. Mater. Electron. 28 (2017) 11832–11845.
[26] V.I. Madogni, B. Kounouhewa, A. Akpo, M. Agbomahéna, S.A. Hounkpatin, C.N. Awanou, Chem. Phys. Lett. 640 (2015) 201–214.
[27] M. Koehl, S. Hoffmann, S. Wiesmeier, Prog. Photovolt. Res. Appl. 25 (2017) 175–183.
[28] Y. Zhang, E. Bovill, J. Kingsley, et al., Sci. Rep. 6 (2016) 21632.
[29] P.A. Troshin, Org. Photon. Photovolt. 3 (2015) 161–182.
[30] V. Turkovic, S. Engmann, D.A.M. Egbe, et al., Sol. Energy Mater. Sol. Cells 120 (2014) 654–668.
[31] H. Hintz, H.-J. Egelhaaf, L. Luer, et al., Chem. Mater. 23 (2011) 145–154.
[32] O. Haillant, D. Dumbleton, A. Zielnik, Sol. Energy Mater. Sol. Cells 95 (2011) 1889–1895.
[33] I. Riedel, J. Parisi, V. Dyakonov, et al., Adv. Funct. Mater. 14 (2004) 38–44.
[34] D. Chen, A.K. Ray, Water Res. 32 (1998) 3223–3234.
[35] P. Atkins, J. Paula, Physical Chemistry, ninth ed., W.H. Freeman, New York, 2010.
[36] J. Kesters, P. Verstappen, J. Raymakers, et al., Chem. Mater. 27 (2015) 1332–1341.
[37] M. Corazza, F.C. Krebs, S.A. Gevorgyan, Sol. Energy Mater. Sol. Cells 143 (2015) 467–472.
[38] N. Bristow, J. Kettle, J. Renew. Sustain. Energy 7 (2015) 013111.
[39] J. Kesters, S. Kudret, S. Bertho, et al., Org. Electron. 15 (2014) 549–562.
[40] R.D. Bettignies, J. Leroy, M. Firon, et al., Synth. Met. 156 (2006) 510–513.
[41] T.J. McMahon, Prog. Photovolt. Res. Appl. 12 (2004) 235–248.
[42] S. Schuller, P. Schilinsky, J. Hauch, et al., Appl. Phys. A 79 (2004) 37–40.
[43] M.A. Arshad, A. Maaroufi, J. Power Sources 391 (2018) 134–147.
[44] M.E. Brown, P.K. Gallagher, Handbook of Thermal Analysis and Calorimetry: Recent Advances, Techniques and Applications, Elsevier B.V, Amsterdam, 2008.
[45] J. Vichova, F. Hartl, A. V. Jr., J. Am. Chem. Soc. 114 (1992) 10903–10910.
[46] M.A. Arshad, A. Maaroufi, G. Pinto, et al., Bull. Mater. Sci. 39 (2016) 1609–1618.
[47] S. Vyazovkin, A.K. Burnham, J.M. Craido, et al., Thermochim. Acta 520 (2011) 1–19.
[48] S. Vyazovkin, Phys. Chem. Chem. Phys. 18 (2016) 18643–18656.
[49] G. Tan, Q. Wang, H. Zheng, J. Phys. Chem. A 115 (2011) 5517–5524.
[50] M.A. Arshad, A. Maaroufi, Thermochim. Acta 585 (2014) 25–35.
[51] J. Sarada, K.V. Nagaraja, Appl. Math. Comput. 217 (2011) 5612–5621.
[52] M.A. Arshad, A. Maaroufi, J. Non.-Cryst. Solids 413 (2015) 53–58.